Phase estimation of a 2D fringe pattern using a monogenic-based multiscale analysis

Mohamed Kaseb, Guillaume Mercère, Hermine Biermé, Fabrice Brémand, Philippe Carré

Phase estimation of a 2D fringe pattern using a monogenic-based multiscale analysis

Mohamed Kaseb, Guillaume Mercère, Hermine Biermé, Fabrice Brémand, Philippe Carré

Phase estimation of a 2D fringe pattern using a monogenic-based multiscale analysis

Mohamed Kaseb[1] Guillaume Mercère[2] Hermine Biermé[3] Fabrice Brémand[4] and Philippe Carré[6]

[1] *Currently with the University of Poitiers, Institut XLIM, 11 Boulevard Marie et Pierre Curie, 86073 Poitiers Cedex 9, France*

[2] *Currently with the University of Poitiers, Laboratoire d'Informatique et d'Automatique pour les Systèmes, 12 rue Pierre Brousse, 86073 Poitiers Cedex 9, France*

[3] *Currently with the University of Poitiers, Laboratoire de Mathématiques et Applications, 11 Boulevard Marie et Pierre Curie, 86073 Poitiers Cedex 9, France*

[4] *Currently with the University of Poitiers, Institut P', 11 Boulevard Marie et Pierre Curie, 86073 Poitiers Cedex 9, France*

[5] *Currently with the University of Poitiers, Institut XLIM, 11 Boulevard Marie et Pierre Curie, 86073 Poitiers Cedex 9, France*

[1] *mohamed.kaseb@univ-poitiers.fr*
[2] *guillaume.mercere@univ-poitiers.fr*
[3] *hermine.bierme@univ-poitiers.fr*
[4] *fabrice.bremand@univ-poitiers.fr*
[5] *philippe.carre@univ-poitiers.fr*

Abstract: In this paper, a multiscale monogenic analysis is applied to 2D interference fringe patterns. The monogenic signal was originally developed as a 2D generalisation of the well-known analytic signal in the 1D case. The analytic and monogenic tools are both useful to extract a phase information, which can then be directly linked with physical quantities. Previous studied have already shown the interest of the monogenic signal in the field of i nterferometry. This paper presents theorical and numerical illustrations of the connexion between the physical phase information and the phase estimated with the monogenic tool. More specifically, the ideal case of pure cosine waves is deeply studied, and then the complexity of the fringe patterns is progressively increased.

One important weakness of the monogenic transform is its singularity at the null frequency, which makes the phase estimations of low frequency fringes diverge. Moreover, the monogenic transform is originally designed for narrowband signals, and encounters difficulties when dealing with noised signals. These problems can be bypassed by performing a multiscale analysis based on the monogenic wavelet transform. Moreover, this paper proposes a simple strategy to combine the information extracted at different scales in order to get a better estimation of the phase. The numerical tests (synthetic and real signals) show how this approach provides a finer extraction of the geometrical structure of the fringe patterns.

1. Introduction

It is well known [1] that, when two waves are superimposed, a new wave that has its own frequency is generated. This phenomenon is called interference [1] and can be observed for all types of waves (sound, light, radio, etc...). In particular, when a network of alternatively opaque and transparent lines is overlaid on another network of similar frequency, a third network of lower frequency appears. This network is called a Moiré pattern [2]. Moiré patterns are of great interest for measuring various dynamical processes like structure deformation because they are purely optical and thus do not require any physical perturbation of the analysed material [3,4]. A network of periodic fringes can be modelled by a luminous intensity function $f : \mathbb{R}^2 \rightarrow \mathbb{R}$,

defined as follows

$$f(\mathbf{x}) = a(\mathbf{x}) + b(\mathbf{x})\cos(\varphi(\mathbf{x})),\ \mathbf{x} = (x_1, x_2) \in \mathbb{R}^2,$$

where $a(\mathbf{x})$ is a direct current term, $b(\mathbf{x})$ the amplitude of the fringe and $\varphi(\mathbf{x})$ its phase at each point (x_1, x_2) of the image [5]. Because the geometrical structure of the fringe network is contained in the phase and can be directly linked with physical quantities of the studied image (like relief and deformation), its estimation is of great importance [4]. Currently, the most widely used techniques are based on phase shifting [6], which consists in generating several fringe patterns by moving one of the two networks. The values of a, b and φ are then extracted point by point using these shifted images (see, e.g., [6] for further details about phase shifting techniques). The main problem of this technique is its lack of practical use when dynamic processes come into play, because it would require several phase shiftings at each time, which is complicated to perform in practice. In order to solve this problem, a phase estimation method based on one single image rather than several images is hence needed. Some previous works have tried to apply signal processing tools like the Fourier and Hilbert transforms to this task, but these 1D techniques show their limits when dealing with complex 2D patterns [7]. Fourteen years ago, a technique requiring only one image, the polynomial Modulated Phase Correlation (pMPC), has been developped in [4] and is more suitable to 2D signals than 1D techniques. This method consists in dividing the image into patches, then fitting the parameters of a fixed model on each patch. Such a procedure can be very time consuming especially when the number of patches is high [4], while a smaller number of patches gives a far less reliable phase estimation. Furthermore, local singularities may appear because of the segmentation, hence the need of a better approach.

New solutions arose when 2D generalisations of the Hilbert transform have been suggested. In [5], Larkin introduced a directional Hilbert transform (called vortex in [5]), and used it to extract the phase of 2D fringe patterns. Later, in [8], Seemantula also provided a good phase extraction technique on 2D fringe patterns based on the Riesz transform and the monogenic signal introduced in [9]. As Larkin said in [5], the monogenic transform is equivalent to his vortex operator. Both [5] and [8] concluded that their respective 2D generalised Hilbert operators were particularly well-suited for slow varying signals, which in terms of the spectrum is equivalent to narrow frequency bands [10]. Larkin went even further and proved that the quality of the monogenic phase extraction decreases with the curvature of the original phase function [5]. During the last decade, the introduction of the monogenic wavelet transform enabled a more refined analysis of 2D signals [11] [12] [13] [14]. These wavelets provide a way to decompose general signals into a combination of narrowband sub-signals on which the Riesz transform can then be applied [15]. The aim of this paper is to give theorical and numerical illustrations of the connection between the physical phase information and the phase estimated with the monogenic tool, then show how the monogenic wavelets improve the Riesz-based phase extraction technique by making it suitable to signals containing low frequency fringes or noise. Moreover, with a simple strategy based on monogenic energy, a signal-adaptative phase estimation is suggested. This multiscale approach was not used in the previous papers dealing with Riesz-based analysis of fringe patterns [5, 8]. Although the mathematical background of this multiscale analysis is the same as in Olhede's [14] work, here it is applied to fringe patterns rather than random fields, and its quality is measured through numerical tests. A comparison of the monogenic phase measure with the pMPC technique is also performed to confirm numerically the relevance of the monogenic tool in the context of interferometry.

This paper is organised as follows. In Section 2, a general presentation of the mathematical concepts and objects necessary to define the monogenic signal and wavelets are given. Then in Section 3 the relevance of the monogenic tool in the context of interferometry is investigated, and numerical illustrations of some theorical properties given in [5] and [8] are performed, a discussion that was not carried out in their studies. Finally, in Section 4 a multiscale analysis

of fringe patterns based on monogenic wavelets is performed to show its benefits compared to Larkin's and Seemantula's works.

2. The monogenic tool

This section introduces the mathematical tools that will allow us to give a proper definition of the local phase in the 1D and 2D cases, respectively, as well as techniques to extract it. Like Larkin did in [5], it is assumed that the direct current (DC) term $a(\mathbf{x})$ is constant and has been removed for the sake of simplicity (for example by resorting to a high pass filter).

2.1. 1D signal

In the 1D case, wave signals can be modelled as follows [10]

$$f(t) = b(t)\cos(\varphi(t)), t \in \mathbb{R}, \tag{1}$$

where $b(t)$ denotes the amplitude of f and $\varphi(t)$ its phase at each instant (or position) t. In practice, f is the only known function, while b and φ have to be estimated from it. In order to reach this goal, the signal f is uniquely extended to the complex domain, then its amplitude and phase are defined as the modulus and argument of this complex signal [10]. By denoting by $\mathcal{F}$ the Fourier transform, the Hilbert transform [16] $\mathcal{H}$ is defined in the Fourier domain as follows

$$\mathcal{F}\{\mathcal{H}f\}(\omega) = H(\omega)\mathcal{F}\{f\}(\omega), \omega \in \mathbb{R}^*, \tag{2}$$

where $H(\omega) = -\mathbf{j}\frac{\omega}{|\omega|}, \omega \in \mathbb{R}^*$. The Hilbert transform could also be defined in the time domain as the convolution product between f and a kernel function h whose Fourier transform is exactly H, but this expression is quite complex and working in the Fourier domain is much more convenient for our application [9]. The complex analytic extension of f is then defined as $f_A(t) = f(t) + \mathbf{j}\mathcal{H}f(t)$ and is called the analytic signal of f [10]. The modulus and argument of f_A, denoted by $a(t)$ and $\phi(t)$ respectively, give an instantaneous measure of amplitude and phase.

2.2. 2D signal

The analytic tool is well known in the signal processing community [10] and is of great interest to detect local features of a signal [17]. The aim now is to generalise it to 2D signals, then use it to define a local amplitude and phase. 2D fringe patterns can be modelled as follows

$$f(\mathbf{x}) = b(\mathbf{x})\cos(\varphi(\mathbf{x})), \mathbf{x} \in \mathbb{R}^2. \tag{3}$$

The Hilbert transform can be generalised in the 2D case by using the Riesz transforms [9] $\mathcal{R}_s$ for $s \in \{1, 2\}$, which are defined in the Fourier domain as follows

$$\mathcal{F}\{\mathcal{R}_s f\}(\omega_1, \omega_2) = -\mathbf{j}\frac{\omega_s}{\sqrt{\omega_1^2 + \omega_2^2}}\mathcal{F}\{f\}(\omega_1, \omega_2), \tag{4}$$

with $(\omega_1, \omega_2) \in \mathbb{R}^2\backslash\{(0, 0)\}$. Again, the Riesz transforms are defined in the frequency domain rather than in the time domain in order to deal with more concise expressions [9]. The 3D signal whose components are f, $\mathcal{R}_1(f)$ and $\mathcal{R}_2(f)$ respectively, is called the monogenic signal of f [9]. The spherical coordinates yield to definition of the monogenic amplitude $a(\mathbf{x})$ and two angular information at each point $\mathbf{x}$, the monogenic phase $\phi(\mathbf{x})$ and the orientation $\theta(\mathbf{x})$ respectively.

Remark

Note that in Equations (1) and (3), the functions b and φ are not unique. For example, for any function $u : \mathbb{R}^2 \rightarrow]0,1]$, $f(\mathbf{x})$ could be written as

$$f(\mathbf{x}) = \tilde{b}(\mathbf{x}) \cos(\tilde{\varphi}(\mathbf{x})), \tag{5}$$

with $\tilde{b}(\mathbf{x}) = \frac{b(t)}{u(\mathbf{x})}$ and $\tilde{\varphi}(\mathbf{x}) = \arccos[u(\mathbf{x}) \cos(\varphi(\mathbf{x}))]$. Consequently, the notions of local amplitude and phase are ambiguous. However, thanks to the monogenic tool, one particular pair of functions b and φ is characterised, yielding an unambiguous notion of local amplitude and phase.
In this section, the whole monogenic theory has been defined for continuous signals. However, in practice, only discrete signals can be processed. This requires the definition of all the previsouly introduced monogenic tools in the discrete domain.

2.3. Discrete monogenic signal

Let $(jT_x, kT_y)_{(j,k)\in\{0,\dots,M-1\}\times\{0,\dots,N-1\}}$ be a 2D grid, with M and N positive integers, T_x and T_y the horizontal and vertical sampling periods respectively. The continuous signal f is then measured at each point of the grid, yielding a 2D discrete signal $f = (f_{j,k})_{j,k}$. Using the 2D discrete Fourier transform defined in [18], the Fourier transform of f, denoted by $F = (F_{j,k})_{j,k}$, can be computed. The Riesz kernel is then applied to F (see [19] and [20] for more details about the way the Riesz kernel is computed), and the discrete Riesz transform of f, denoted by $\mathcal{R}f$, is obtained by reversing the 2D discrete Fourier transform [18]. Since F is not symmetric, meaning that it does not satisfy $F(-\omega) = \overline{F(\omega)}$, $\mathcal{R}f$ is a complex signal. The three components of the discrete monogenic signal of f are then f itself, the real part of $\mathcal{R}f$ and its imaginary part respectively. The discrete amplitude, phase and orientation are finally computed from these three components.
At this point, no new mathematical notion has been introduced. The notions of amplitude and phase defined previously, as well as their dicretisation, are totally in line with the works of both Larkin [5] and Seemantula [8]. However, in these previous studies the monogenic tool was applied on fringe patterns directly, without taking into account the frequency band where the fringes lie. As seen in Section 2.2, the Riesz transform is not defined at the null frequency, and Section 4 shows how this singularity alters the phase estimation of low frequency fringes. Furthermore, random perturbations may also cause the quality of the estimation to drop as Section 3 shows it. The Bidimensional Empirical Mode Decomposition (BEMD) introduced in [21] was specifically designed to bypass these diffculties. This technique is used to extract the different modes of a signal, on which the monogenic transform is then applied, but requires complex operations like interpolation. Another approach is Unser's multiscale analysis based on wavelets [22], which relies on filterbanks to decompose the signal and is hence numerically more simple. Here this multiscale approach is applied to fringe patterns. The monogenic wavelets that enable this multiscale analysis are introduced in the next Sub-Section.

2.4. Monogenic wavelets

The amplitude, phase and orientation of the monogenic signal can be interpreted as a measure of energy, geometrical structure and main direction respectively [9]. An important condition for this model to be valid is that the signal has to be narrowband [8, 10]. A first reason comes from the meaning of *phase* that indicates oscillation. Another reason is the mathematical constraint of the Hilbert and Riesz transforms having a singularity at $\omega = 0$ in the Fourier domain - which excludes all signals having low frequency energy. Finally, random perturbations occurring in the signal may cause the frequency range to become too wide for a monogenic analysis.
This clearly suggests using the monogenic analysis in a multiscale manner through some subband decomposition in order to handle non-narrowband signals as well. In 2009, a monogenic wavelet

transform was proposed in [11] ans [14], that is specially defined for 2D signals. The scheme of [11] performs multiresolution monogenic analysis by using two parallel filterbanks : one 'primary' transform tied to a real continuous wavelet frame and a so-called 'Riesz-Laplace' wavelet transform tied to a complex frame. Multiresolution analyses are built from the nearly isotropic polyharmonic B-spline of [23].
The wavelet for the 'primary' decomposition ψ is a Mexican hat-like nearly isotropic function and the 'Riesz-Laplace' wavelet $\psi^{\mathcal{R}}$ is derived from it (in the Fourier domain) as follows

$$\psi^{\mathcal{R}} \overset{\mathcal{F}}{\longleftrightarrow} \frac{\mathbf{j}\omega_1 + \omega_2}{\|\omega\|}\hat{\psi}(\omega). \tag{6}$$

For $i \in \mathbb{N}$ and $\mathbf{m} \in \mathbb{Z}^2$, let $\psi_{i,\mathbf{m}}(\mathbf{x}) = 2^i\psi(2^i\mathbf{x} - \mathbf{m}/2)$ be the scaled and shifted version of ψ (same for $\psi^{\mathcal{R}}$). From these functions, by denoting ψ_i for $\psi_{i,0}$, the following decomposition can be defined:

$$c_{i,\mathbf{m}} = \left\langle s, \psi_{i,\mathbf{m}} \right\rangle = (\psi_i * s)\,(2^{-(i+1)}\mathbf{m}), \tag{7}$$

$$d_{i,\mathbf{m}} = \left\langle s, \psi^{\mathcal{R}}_{i,\mathbf{m}} \right\rangle = \{\mathcal{R}\,(\psi_i * s)\}(2^{-(i+1)}\mathbf{m}), \tag{8}$$

where $\langle ., . \rangle$ and $*$ denote the scalar and the convolution product in $L^2(\mathbb{R}^2)$, respectively. These wavelet coefficients form an exact monogenic signal at each scale. For all $i \in \mathbb{N}$ and $\mathbf{m} \in \mathbb{Z}^2$, $c_{i,\mathbf{m}} \in \mathbb{R}$ and $d_{i,\mathbf{m}} \in \mathbb{C}$ are merged into 3-vectors and turned into spherical coordinates as presented in Section 2.2, and the wavelet coefficients contain the same physical information (energy, geometrical structure and orientation) as the monoscale monogenic representation but at different scales of the image.
The original work of Unser uses a pyramid-like dyadic subsampling scheme, which is justified by the need of a little redundancy and "tight frame" condition [11]. However in our work, the undecimated design will help us to precisely analyze the phase information through the scales. This is why we propose to release the tight constraint for an undecimated scheme.
Because the essential action of the Riesz transform is a pure phase-shifting operation, the low-pass and high-pass filters H_i and G_i are required to be perfectly neutral with respect to the signal's phase. Their frequency response must then be radial, positive and real-valued. The filterbank is efficiently computed in the FFT domain with a global linear computational complexity [22]. The wavelet design for our purpose is introduced in [15] and [19].
Contrary to what Larkin and Seemantula did in [5] and [8], we do not apply the Riesz transform on the signal f directly, but rather decompose it in a set of L narrowband sub-signals $f^{(i)}$ ($i = 1, \dots L$, $L \in \mathbb{N}^*_+$) on which the Riesz transform is better defined. Each sub-signal $f^{(i)}$ corresponds to the information contained in the original signal f at the frequency band $[2^{-(i+1)}; 2^{-i}]$, and can be written in the spherical coordinates as $(a^{(i)}, \phi^{(i)}, \theta^{(i)})$. Furthermore, using the energy information provided by the monogenic amplitude $a^{(i)}$, the information contained in the different scales are combined in order to get a better estimation of the phase. At each pixel (j, k), the scale i for which the amplitude is maximal is selected. Hence, the phase value at (j, k) is given by

$$\phi_{j,k} = \phi^{(i_0)}_{j,k}, \text{ with } i_0 = \underset{i=1,\dots,L}{\arg\max}\{a^{(i)}_{j,k}\}. \tag{9}$$

3. Properties of the monogenic tool and synthetic tests

As explained in the previous section, the monogenic amplitude and phase functions are not the only pair of functions b and φ satisfying Equation (3). Therefore, if a signal is generated from a particular choice of functions b and φ, there is apparently no reason for the measured monogenic phase ϕ to coincide with φ. Both [5] and [8] gave certain conditions under which the monogenic phase ϕ matches the physical phase φ and extracts the expected geometrical structure of the

fringes. These conditions were then illustrated by highlighting the visual similarity between the original fringe patterns and their respective computed monogenic phases. In this section, further numerical details about this "similarity" are given by doing numerical comparisons between the physical phase, used to generate the signal, and the monogenic phase computed from the signal.

3.1. A numerical measure of similarity

Let $b = (b_{j,k})_{j,k}$ and $\varphi = (\varphi_{j,k})_{j,k}$ denote the discrete physical amplitude and phase of the signal f respectively, and $\phi = (\phi_{j,k})_{j,k}$ the discrete monogenic phase defined in the previous paragraph. As said before, the question is how close the measured monogenic phase ϕ stands from φ, hence the need of a numerical measure of similarity between two discrete signals. It should also not be forgotten that the phase information is an angle defined modulo 2π. Values like $-\pi + \epsilon$ and $\pi - \epsilon$ (ϵ being a small positive real number) may thus be deemed as highly different while they hold the same angular information. Comparing the cosine of the phase values instead of the phase values directly is a good way to bypass this difficulty. In this paper, numerical comparisons are performed using the Best Fit (BFT) defined in [24] and the Variance Accounted For (VAF) defined in [25], which are calculated as follows

$$\begin{cases} \mathrm{BFT}(\varphi,\phi) = \max\{100(1 - \frac{\|\cos\phi - \cos\varphi\|_2}{\|\cos\varphi - \overline{\cos\varphi}\|_2}), 0\}, \\ \mathrm{VAF}(\varphi,\phi) = \max\{(100(1 - \frac{V(\cos\phi - \cos\varphi)}{V(\cos\varphi)}), 0\}, \end{cases} \tag{10}$$

where for all $M \times N$ matrix A,

- $\|A\|_2^2 = \sum_{j=0}^{M-1} \sum_{k=0}^{N-1} A_{j,k}^2$,
- $\overline{A} = \frac{1}{MN} \sum_{j=0}^{M-1} \sum_{k=0}^{N-1} A_{j,k}$,
- $V(A) = \frac{1}{MN}\|A\|_2^2 - \overline{A}^2$.

The BFT and VAF criteria should be interpreted as a bias and variance information respectively, which is very instructive when testing an estimation technique. Histograms and quantiles of the cosine error $\cos(\phi - \varphi)$ are also used to determine how this error is distributed on the image. Note that both BFT and VAF are not defined for constant signals, but these are obviously out of the scope of this study. Before dealing with real fringe patterns, the monogenic tool is first applied to the special case of pure cosine waves, which are in both 1D [10] and 2D [5, 8] cases the most canonical signals from the analytic/monogenic point of view.

3.2. Pure cosine wave

A 1D signal is a pure cosine wave if it has a constant amplitude and a linear phase, that is

$$f(t) = b_0 \cos(\omega t), \tag{11}$$

with $t \in \mathbb{R}$, and both $b_0 > 0$ and $\omega > 0$. Its Hilbert transform (see [10], Chapter 2) is given by

$$\mathcal{H}f(t) = b_0 \sin(\omega t), \tag{12}$$

which implies, using the previously introduced notations, that

$$\phi(t) = \varphi(t) = \omega t. \tag{13}$$

Pure cosine waves are generalised to the 2D case as follows

$$f(\mathbf{x}) = b_0 \cos(\mathbf{k}^T \mathbf{x}), \tag{14}$$

where $\mathbf{k} = \omega(\cos\alpha, \sin\alpha)^T$ is the wave vector and $\mathbf{x} = (x_1, x_2)^T$ the position respectively [26]. The Riesz transforms of such a signal are given by [8, 26]

$$\begin{cases} \mathcal{R}_1 f(\mathbf{x}) = b_0 \sin(\mathbf{k}^T\mathbf{x})\cos\alpha, \\ \mathcal{R}_2 f(\mathbf{x}) = b_0 \sin(\mathbf{k}^T\mathbf{x})\sin\alpha. \end{cases} \tag{15}$$

The monogenic signal of f has thus two spherical representations $(b_0, \mathbf{k}^T\mathbf{x}, \alpha)$ and $(a(\mathbf{x}), \phi(\mathbf{x}), \theta(\mathbf{x}))$ as defined previously. By identification of the spherical coordinates term by term, both monogenic and physical definitions of phase can be identified due to the uniqueness of the spherical coordinates, hence

$$\phi(\mathbf{x}) = \varphi(\mathbf{x}) = \mathbf{k}^T\mathbf{x}. \tag{16}$$

Of course this equality does not imply that Equation (14) is the unique way to express f as $b(\mathbf{x})\cos(\varphi(\mathbf{x}))$. What this equation says is that applying the monogenic tool to a pure cosine waves will always give a constant amplitude and a linear phase. Note that the monogenic orientation defined in the previous section is exactly the angle α, which in the case of a cosine wave is constant.

In both [5] and [8], a theorical study of pure cosine waves was already performed in both 1D and 2D cases, leading to the same conclusion as ours. In this paper, these properties are illustrated with numerical simulations, something which was not carried out in the previous works. The cosine wave is computed on a discrete square grid $(jT_x, kT_y)_{(j,k)\in\{0,\dots,N-1\}\times\{0,\dots,N-1\}}$, as follows

$$f_{j,k} = b_0 \cos[2\pi f_0(jT_x\cos\alpha + kT_y\sin\alpha)], \tag{17}$$

with $f_0 = \frac{N_0}{N}$ and N_0 an integer. This ensures that the signal contains an integer number of periods, hence avoiding edge-mismatching. The monogenic tool is then applied to a cosine wave generated with $T_x = T_y = 0.1$, $N = 100$, $b_0 = 0.5$, $N_0 = 20$ and $\alpha = \frac{\pi}{4}$ respectively. Note that T_x and T_y have been chosen small enough to fit the Shannon-Nyquist bound. The identification of the physical and monogenic phases is numerically confirmed as can be seen in Figure 1, which shows a 2D cosine wave, its physical phase $\mathbf{k}^T\mathbf{x}$ and the monogenic phase calculated using the 2D Fast Fourier Transform. The white zones correspond to values close to $-\pi$ while the black zones correspond to values close to π. The monogenic and physical phase look very close, and this is confirmed by the very high values of BFT and VAF, 99, 58% and 100% respectively. Furthermore, 99.44% of the cosine error values $\cos(\phi - \varphi)$ are higher than 0.999, and almost 100% are higher than 0.99, which shows how ϕ and φ are close. This gives a good numerical illustration of what Larkin [5] and Seemantula [8] had theorically proved in their respective studies.

Because pure cosine waves correspond to parallel fringes, the frequency is constant in the whole image. Consequently, if a multiscale analysis is performed, all the information of the signal should be contained in one single frequency band $[2^{-(i+1)}; 2^{-i}]$. In this particular case, the numerical frequency is constantly equal to $f_0T_x = f_0T_y = 0.02$, and thus lies in the frequency band associated with the scale $i = 5$, *i.e.*, $[2^{-6}; 2^{-5}]$ (approximately $[0.0156; 0.0313]$). Figure 2 shows the phase (left) and amplitude (right) obtained by applying the monogenic wavelet transform to a cosine wave at six scales. The highest values of both amplitude and phase correspond to the white zones. Because the amplitude gives a measure of the local energy of the signal, the frequency band in which this energy is maximal indicates that the fringes lie in this particular band. In this example, the maximal energy corresponds to scale $i = 5$, which is exactly what was expected. Working at different scales does not have any impact on the estimation of the phase, which is in all cases well estimated. This shows that the straightforward monogenic analysis defined in [5] and [8] is enough when dealing with cosine waves.

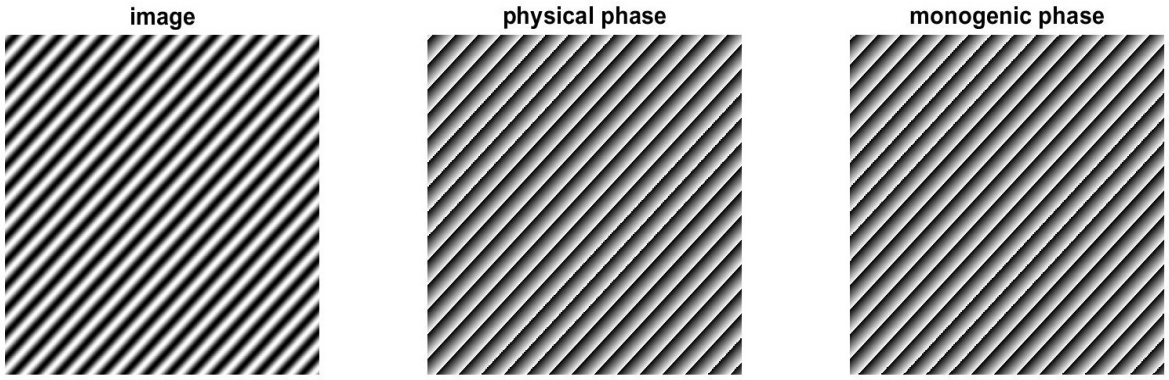

Fig. 1. Phase estimation of a 2D cosine wave

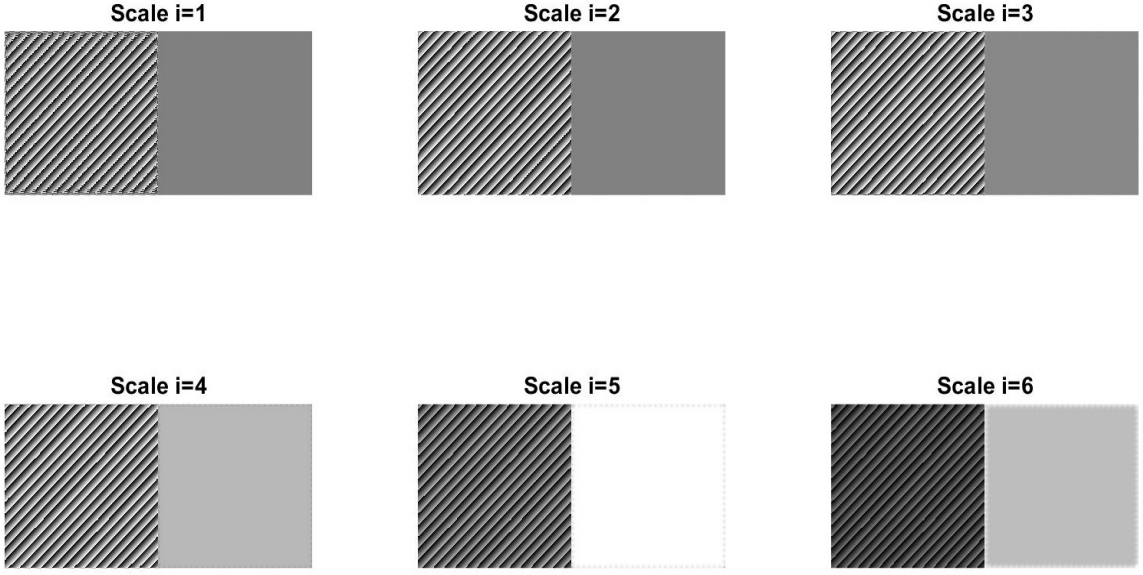

Fig. 2. Phase estimation of a 2D cosine wave at different scales. Phase (left) and amplitude (right)

The next paragraph deals with more complex patterns and gives some details about the importance of having slow varying signals.

3.3. Parabolic chirp

The previous section has shown that the monogenic phase estimation technique gives very good results when dealing with pure cosine waves, *i.e.*, signals with constant amplitude and linear phase. However, this model is not enough to deal with the more complex fringe patterns studied in the last section of this paper. In the case of 1D signals, one natural way of increasing the complexity of the phase is to assume it quadratic rather than linear, while the amplitude stays constant. This is indeed the first example of 1D non cosine wave introduced in [10]. Such a wave is called a parabolic chirp, modelled as

$$f(t) = \cos(a^2 t^2), \tag{18}$$

with $a > 0$. Its Hilbert transform is given by

$$\mathcal{H}f(t) = \sqrt{\frac{2}{\pi}}[A(t)\sin(a^2t^2) + B(t)\cos(a^2t^2)], \tag{19}$$

with $A(t)$ and $B(t)$ two functions verifying $A(\infty) = \sqrt{\frac{\pi}{2}}$ and $B(\infty) = 0$ respectively (again, see [10] for further details). When t tends to infinity, $\mathcal{H}f(t)$ is equivalent to $\sin(a^2t^2)$, which implies that the physical and monogenic phases are asymptotically equal. The parabolic chirp can be generalised in the 2D case as

$$f(\mathbf{x}) = b_0 \cos[a^2(x_1^2 + x_2^2)]. \tag{20}$$

Because the phase is not linear anymore, the monogenic phase is not equal to the original quadratic phase. However, Larkin has proved in [5] that the phase estimation error $\Delta\phi(\mathbf{x})$ is directly linked with the curvature of the phase function. Applying the equation he gave in [5] to 2D parabolic chirp yields to

$$\Delta\phi(\mathbf{x}) \approx \frac{1}{2a^2||\mathbf{x}||^2}. \tag{21}$$

Hence, when a or $||\mathbf{x}||$ increase, the phase estimation error decreases. In other words, 2D parabolic chirps behave asymptotically as cosine waves, and the similarity between the estimated monogenic phase ϕ and the physical phase φ also increases for greater values of the a parameter. This stands totally in line with Picinbono's work in the 1D case [10]. Note that, contrary to the case of pure cosine waves, the local frequency of parabolic chirps increases with $||\mathbf{x}||$. Consequently, when generating a parabolic chirp, it is impossible to choose a sampling period that avoids aliasing on the whole image. The size of the image must hence be reduced when a increases in order to avoid such a sampling problem. Figure 3 shows how the similarity (in cosine) between the computed monogenic phase and the original quadratic phase increases with a, confirming what Equation (21) was suggesting. Figure 4 gives an example of a 2D parabolic chirp with $a = 0.2$ (the discretisation parameters being the same as in Section 3.2), its physical phase ans its estimated monogenic phase. Both phases look alike except at the top left corner. The BFT and VAF criteria are equal to 92.13% and 99.38% respectively, which is very satisfactory. Furthermore, 96.18% of the cosine error values are higher than 0.99, and 98.45% are higher than 0.95, which is not as high as in the linear case, but still very close to 1.

Because the frequency of the fringes increases with $||\mathbf{x}||$, the energy is not contained in a single frequency band. Figure 5 shows the phase (left) and amplitude (right) obtained by applying the monogenic wavelet transform to a parabolic chirp at six scales. Most of the signal lies at scale $i = 4$, except for the top left corner which lies in lower frequency bands ($i = 5$ and $i = 6$).

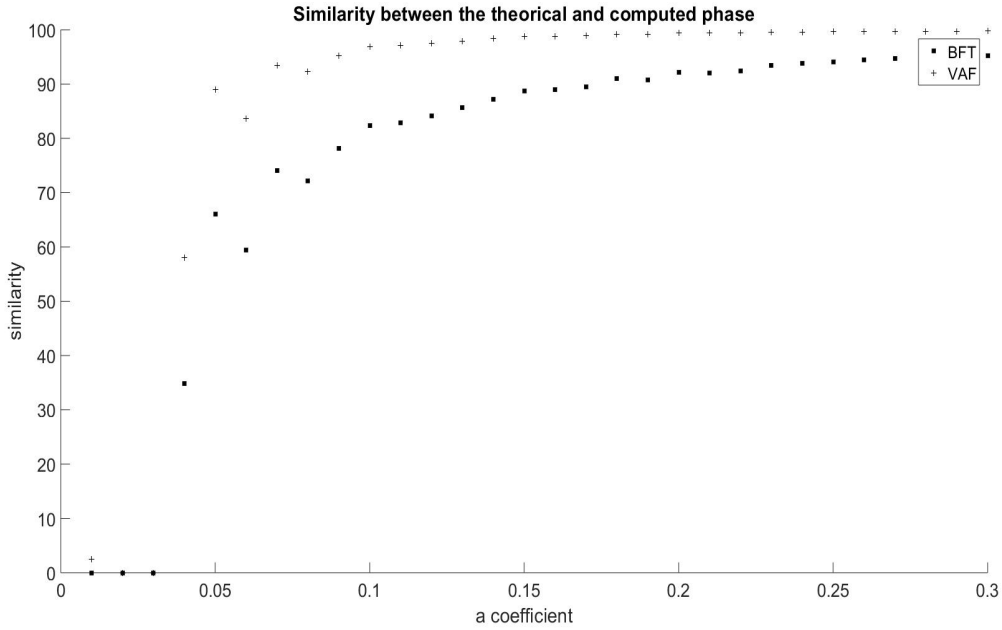

Fig. 3. Influence of the a parameter on the quality of the estimation

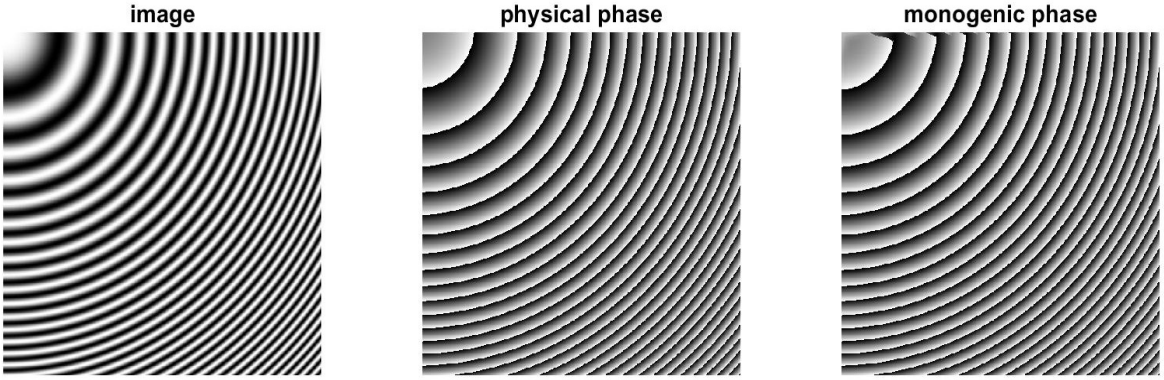

Fig. 4. Phase estimation of a 2D parabolic chirp

Using Equation (9), a new estimation for the phase is obtained, which is represented in Figure 6 along with the original phase and the straightforward monogenic phase. Both techniques give similar results, the straightforward approach performing slightly better according to the BFT and VAF criteria ($BFT = 92.13\%$ and $VAF = 99.38\%$ for the straightforward monogenic phase, $BFT = 90.97\%$ and $VAF = 99.18\%$ for the multiscale monogenic phase). These good results confirm that Riesz-based estimation techniques perform well on cosine waves and parabolic chirps, and does not need multiscale analysis to be improved. The next section gets further away from the ideal case of cosine waves and deals with a more complex fringe pattern to illustrate the benefits of the multiscale analysis.

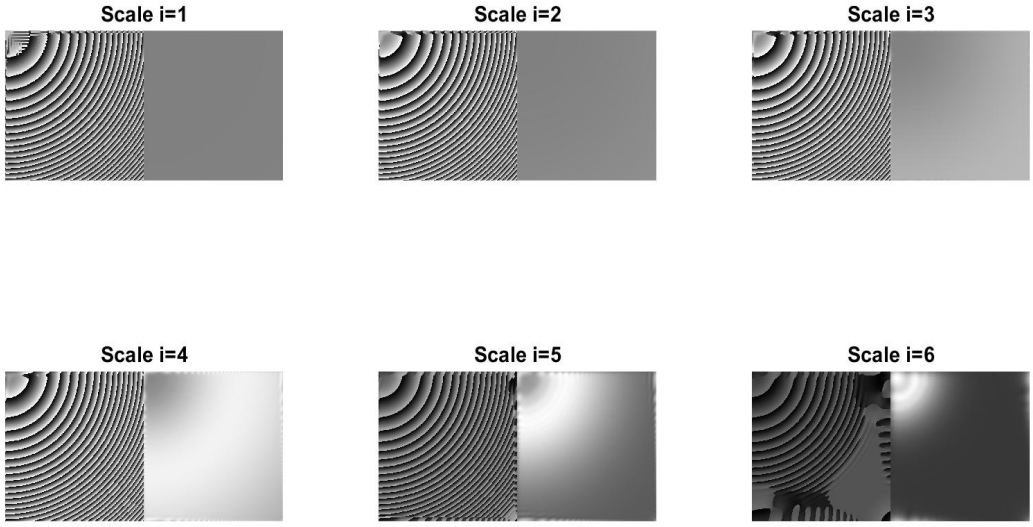

Fig. 5. Phase estimation of a parabolic chirp at different scales. Phase (left) and amplitude (right)

3.4. Influence of noise on the phase estimation

As explained in Section 2.4, the monogenic transform is well-suited for narrowband signals, while the multiscale approach has been designed to better deal with signals that do not fit this property. Therefore, the phase of noised signals is more likely to be well estimated by a multiscale approach than by a monoscale one. This section aims at illustrating this asumption. Let $f = (b_{j,k} \cos \varphi_{j,k})_{j,k \in \{0,\dots M-1\} \times \{0,\dots N-1\}}$ be a discrete 2D signal and $\epsilon = (\epsilon_{j,k})_{j,k \in \{0,\dots M-1\} \times \{0,\dots N-1\}}$ a 2D Gaussian white noise with variance σ^2. Applying the monogenic tool to the noised signal $\tilde{f} = f + \epsilon$ yields to a noised estimation of the phase, denoted by $\tilde{\phi}$. It is then possible to determine how far $\tilde{\phi}$ stands from the physical phase φ by using the BFT and VAF criteria.

The straightforward and multiscale monogenic estimation techniques are now applied to the same cosine wave and parabolic chirp as those studied in Section 2.2 and 2.3, respectively. Figure 7 and 8 show how the similarity criteria between the noised estimated phase and its theorical

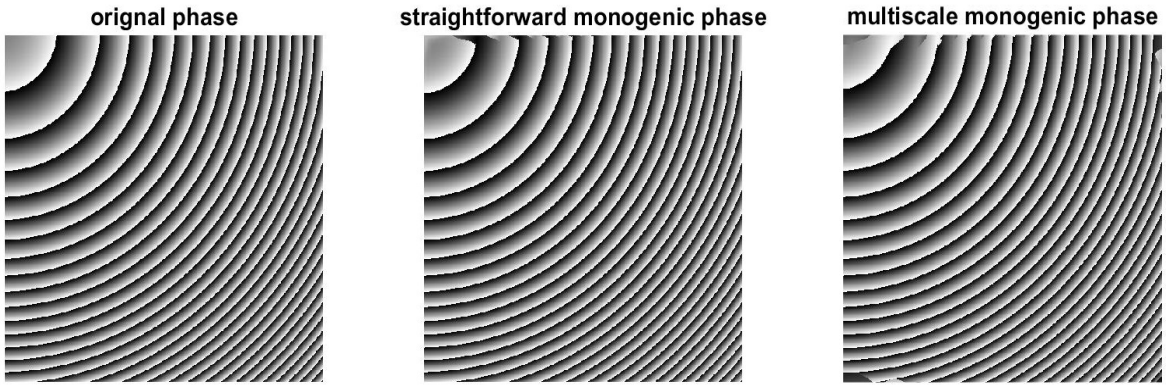

Fig. 6. Original image (left), straightforward monogenic phase (centre) and multiscale monogenic phase (right)

counterpart is affected by the standard deviation of the noise σ, for both techniques and both signals. As expected, the quality of the estimation drops when the noise becomes too important, but this decrease occurs much later when applying the multiscale analysis. Both BFT and VAF reach 0% when σ exceeds 0.05 in the monoscale case, while they still have high values when $\sigma = 1$ ($BFT \approx 90\%$, $VAF \approx 100\%$). This gives a good illustration of how the multiscale approach deals better with noised signals.

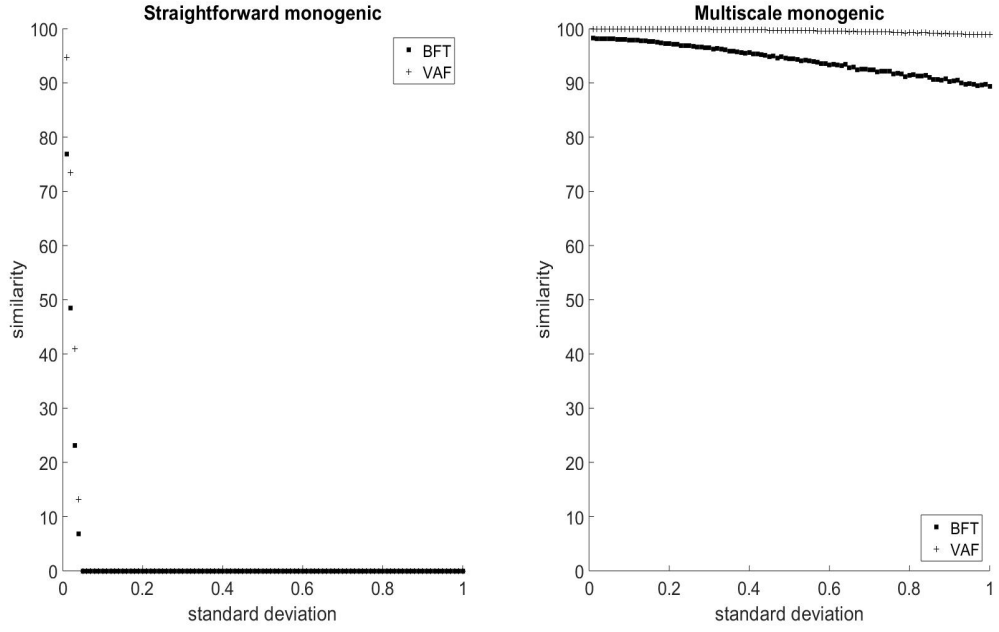

Fig. 7. Influence of noise on the quality of the estimation (cosine wave)

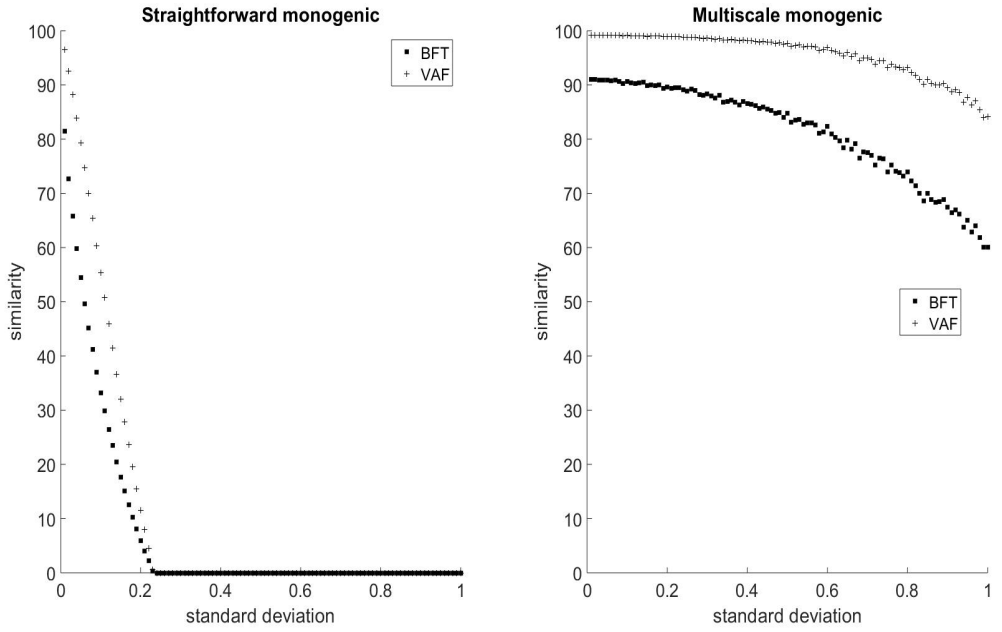

Fig. 8. Influence of noise on the quality of the estimation (parabolic chirp)

4. Application to 2D fringe patterns

In this section, a numerical comparison is performed between the phase computed by the monogenic estimation with its physical counterpart in cases when mathematics cannot ensure their identification, *i.e.*, the signals are neither pure nor asymptotic cosine waves. These results are then compared with those given by the pMPC method previously developed in [4]. In the pMPC procedure, the image is first divided into patches of equal size and an *a priori* model is chosen for the amplitude and phase of the fringes located inside the patches. At each patch, several fringe patterns are generated (with different parametrisations depending on the chosen model) and the closest to the original fringes according to statistical correlation is selected.

4.1. Concentric circular fringes

The most canonical example treated in [4] was the case of concentric circular fringes. These fringes are modelled by a constant amplitude and a phase defined by

$$\varphi(\mathbf{x}) = \frac{2\pi}{p}\sqrt{(x_1 - x_1^c)^2 + (x_2 - x_2^c)^2}, \tag{22}$$

where $p > 0$ denotes the interfringe and $(x_1^c, x_2^c) \in \mathbb{R}^2$ are the coordinates of the central pixel of the image. In practice, such fringes may correspond to level sets on a spherical dome [4]. After generating a discrete sample of concentric circular fringes, the straightforward and multiscale monogenic procedures are applied, then the local phase is computed at each point, and compared with the phase obtained by the pMPC in [4]. Figure 9 shows the estimated phases obtained by the pMPC, straightforward monogenic, multiscale monogenic techniques. All three techniques perform well, but the monogenic approaches give better results at the center of the image. In Figures 10, the histograms show that the monogenic estimation cosine error stays very close to 1, especially with multiscale analysis, while the pMPC error can take lower values.

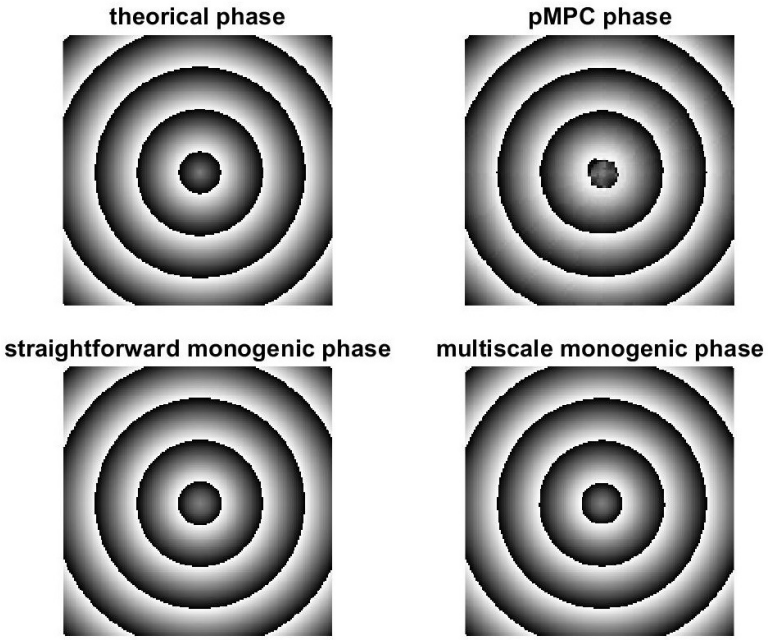

Fig. 9. Theorical (top left), pMPC (top right), straightforward monogenic (bottom left) and multiscale monogenic phase (bottom right)

Table 1 gives a numerical confirmation of these qualitative observations. The multiscale monogenic estimation gives the highest values of BFT and VAF, followed by the straightforward monogenic estimation and then the pMPC. Besides the improved similarity, the monogenic estimation techniques (with or without multiscale analysis) require neither the choice of an *a priori* model for the phase, nor segmentation of the image. Consequently, they rely much less on human choices and perform more automatically.

	pMPC	straightforward monogenic	multiscale monogenic
BFT	80.56%	90.82%	95.25%
VAF	96.23%	99.16%	99.78%

Table 1. Similarity between the theorical and computed phases

4.2. Application of a real pattern

In the previous case, the monogenic phase estimation has proved its relevance beyond the ideal case of cosine waves. Besides, the multiscale analysis has improved the already good results of the straightforward monogenic approach. These procedures are now applied to a real fringe pattern, and then compare the results to the phase estimated by the pMPC in [4]. The comparision can only be qualitative since the "theorical" phase is unknown. As can be seen in Figure 11, the lower part of the image is well estimated while, in the upper part, the straightforward monogenic technique fails to extract the structure of the image. The pMPC however works the same way in every part of the image. As seen earlier, the Riesz operator has a singularity at the zero-frequency, and numerical problems happen when dealing with low frequency fringes, which is the case in

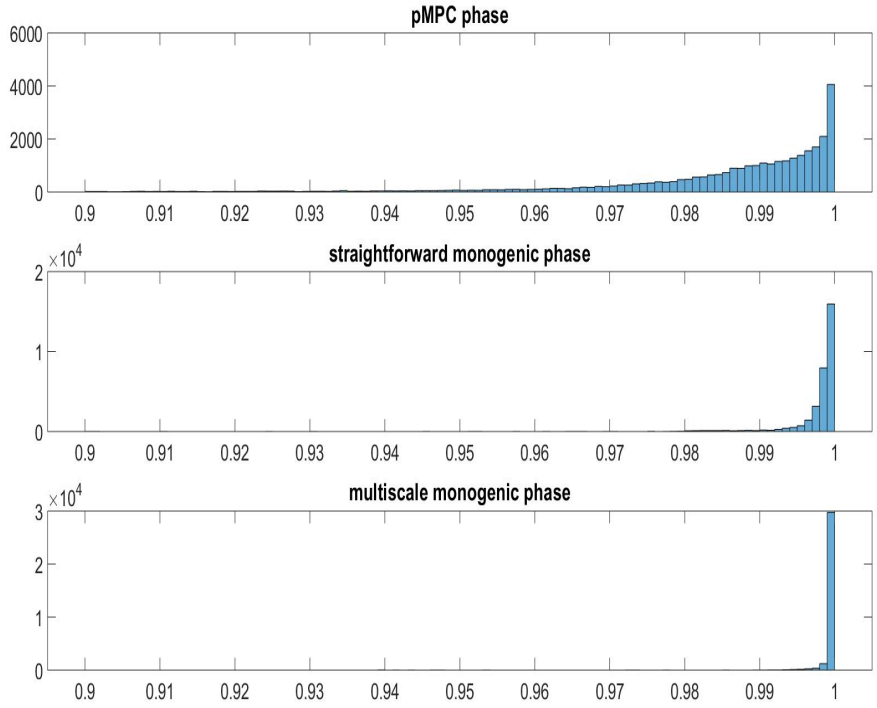

Fig. 10. pMPC (top), straightforward monogenic (centre) and multiscale monogenic (bottom)

the upper half of the image. The multiscale analysis, applied with $L = 3$, performs better in this zone, even though the estimation is heavily disturbed near the borders. Figure 12 shows that the straightforward and multiscale monogenic tools both extract the finer details of the circular fringes better than the pMPC. This confirms that the monogenic tool can provide a precise estimation of the phase, which is totally in line with Larkin's and Seemantula's works. The multiscale analysis, which was not performed in neither of these two studies, enables the monogenic tool to better extract the phase when the frequency band of the fringes slows down and makes the Riesz operator diverge. Furthermore, it is more suitable to non-narrowband signals, particularly noised signals. In Figure 13, the monogenic tools are applied to another fringe patterns. Again, the straightforward and multiscale monogenic estimations both give good results, but the multiscale analysis makes the final phase estimation smoother, especially in zones where the frequency of the fringes is low. This illustrates how the multiscale approach based on wavelets improves the monogenic estimation of the phase.

Remember that the local phase is computed using the spherical coordinates, and is thus only known modulo 2π. However, in the case of fringe patterns, two different phases that share the same principal value are not associated with the same physical quantities [27]. For example, if two adjacent pixels are associated with the phase values $\pi + \epsilon$ and $\pi - \epsilon$ respectively (ϵ being a very small but strictly positive number), an abrupt jump will appear in the phase while in fact their respective phase values are very close. This constitutes the phase unwrapping problem, and an essential part of fringe analysis, but it is out of the scope of this paper.

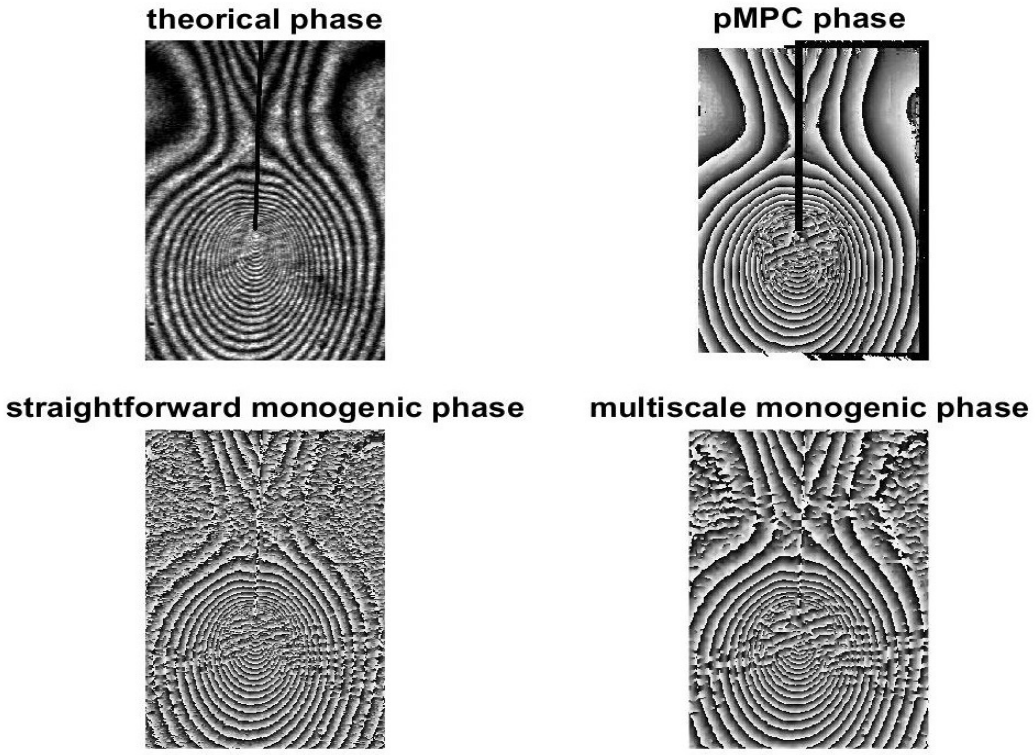

Fig. 11. Original image (top left), pMPC (top right), straightforward monogenic (bottom left) and multiscale monogenic phase (bottom right)

Fig. 12. pMPC (left), straightforward monogenic (centre) and multiscale monogenic phase (right)

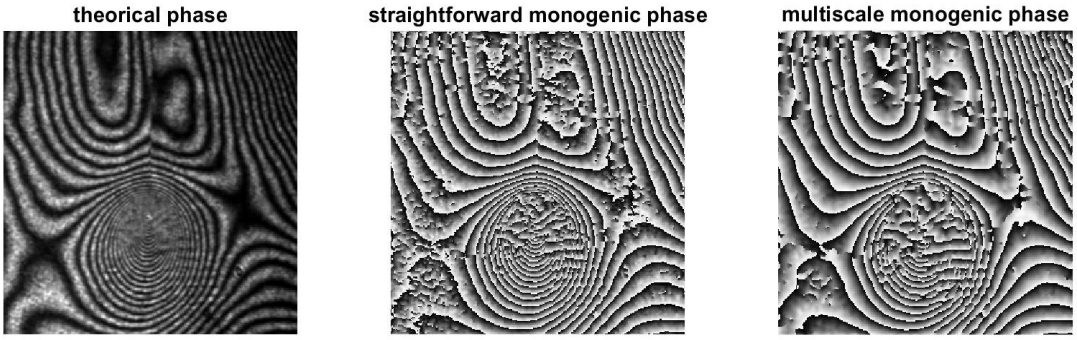

Fig. 13. Original image (left), straightforward monogenic (centre) and multiscale monogenic phase (right)

5. Conclusion and perspectives

Similarly to the analytic signal of the 1D case, the monogenic signal gives a proper, unambiguous notion of local amplitude and local phase in the case of 2D wave signals. The monogenic phase defined this way can be computed just from one single image and does not require any segmentation contrary to the MPC while being much faster. While Larkin and Seemantula had already illustrated this fact, this paper strenghtens it by giving numerical comparisons between the MPC and monogenic phase extraction techniques. Furthermore, this paper introduces a multiscale approach based on monogenic wavelets which had not been used in the previous studies dealing with Riesz-based analysis of fringe patterns [5, 8]. This technique provides a finer extraction of the phase in the case of more complex fringe patterns with low frequency zones or random perturbations, a fact that has been illustrated both theorically and numerically.

The analytic signal has been the subject of much theorical and numerical studies in the second half of the 20th century [10]. Now that a consistent 2D notion of phase has been defined thanks to the Riesz transform, there are lots of interesting results that could be generalised to 2D signals in order to have a better idea of the geometrical information extracted by the monogenic tool when the signal is not a pure cosine wave.

One other important issue that has not been treated in this study is the inherent periodicity of the phase, the so-called phase unwrapping problem evoked at the end of Section 4.2. Various techniques have been developped to solve this problem [27, 28], but none of them works perfectly, and few have yet been applied to a monogenic phase.

Finally, as it would be irrealistic to model any structure with deterministic equations, later studies will have to include stochastic elements. Looking at how random perturbations affect the estimation of the phase and what properties can be extracted from a randomly distributed phase stand among the main axes of reflexion.

References

1. W. H. Steel, *Interferometry, second Edition: Cambridge Studies in Modern Optics 1* (Cambridge University Press, 1986).
2. M. G. L. Gustafsson, "Surpassing the lateral resolution limit by a factor of two using structured illumination microscopy," J. Microsc. **198**, 82–87 (2000).
3. R. D. W., *Interferogram analysis, digital fringe pattern measurement techniques* (CRC Press, 1993).
4. E. Robin, V. Valle, and F. Brémand, "Phase demodulation method from a single fringe pattern based on correlation with a polynomial form," Appl. Opt. **44**, 7261–7269 (2005).
5. K. G. Larkin, D. J. Bone, and M. A. Oldfield, "Natural demodulation of two-dimensional fringe patterns," J. Opt. Soc. Am. **18**, 1862–1881 (2001).

6. J. M. Bruning, D. R. Herriott, J. E. Gallagher, D. P. Rosenfeld, A. D. White, and D. J. Bragaccio, "Digital wavefront measuring interferometer for testing optical surfaces and lenses," Appl. Opt. **13**, 2693–2703 (1974).
7. Y. Morimoto, Y. Seguchi, and T. Higashi, "Two-dimensional moiré method and grid method using Fourier transform," Exp. mechanics **29**, 399–404 (1989).
8. C. S. Seelamantula, N. Pavillon, C. Depeursinge, and M. Unser, "Local demodulation of holograms using the Riesz transform with application to microscopy," J. Opt. Soc. Am. **29**, 2118–2129 (2012).
9. M. Felsberg, "Low-level image processing with the structure multivector," Ph.D. thesis, University of Kiel (2002).
10. B. Picinbono, *Time-frequency analysis* (ISTE Ltd and John Wiley & Sons, Inc, 2008).
11. M. Unser, "Multiresolution monogenic signal analysis usingthe Riesz–Laplace wavelet transform," IEEE Transactions on Signal Process. (2009).
12. S. Olhede and G. Metikas, "Multiple monogenic morse wavelets," IEEE Transactions on Signal Process. **55** (2007).
13. J.Cnops, "The wavelet transform in clifford analysis," Comput. Methods Funct. Theory **1**, 353–374 (2001).
14. S. Olhede and G. Metikas, "The monogenic wavelet transform," IEEE Transactions on Signal Process. **57** (2009).
15. R. Soulard and P. Carré, "Elliptical monogenic wavelets for the analysis and processing of color images," IEEE Transactions on Signal Process. **66** (2015).
16. M. Johansson, "The Hilbert transform," Ph.D. thesis, University of Växjö (2013).
17. B. .Boashash, "Estimating and interpreting the instantaneous frequency of a signal-Part I: Fundamentals," Proc. IEEE **80**, 519–538 (1992).
18. W. Burger and M. J. Burge, *Digital image processing* (Springer, London, 2008).
19. R. Soulard and P. Carré, "Characterization of color images with multiscale monogenic maxima," IEEE Transactions on Pattern Analysis Mach. Intell. **PP** (2017).
20. P. Carré and R. Soulard, "Color image processing with the elliptical monogenic wavelets representation," http://xlim-sic.labo.univ-poitiers.fr/projets/colormonogenic/chap1b.php.
21. J. C. Nunes, S. Guyot, and E. Deléchelle, "Texture analysis based on local analysis of the bidimensional empirical mode decomposition," Mach. Vis. Appl. **16**, 177–188 (2005).
22. M. Unser and N. Chenouard, "A unifying parametric framework for 2d steerable wavelet transforms," SIAM J. on Imaging Sci. **6** (2013).
23. D. VandeVille, T. Blu, and M. Unser, "Isotropic polyharmonic B-splines: scaling functions and wavelets," IEEE Transactions on Signal Process. (2005).
24. L. Ljung, "System identification toolbox for use with Matlab," https://www.researchgate.net/publication/37405937_System_Identification_Toolbox_for_use_with_MATLAB (2011).
25. M. Verhaegen and V. Verdult, *Filtering and system identification : a least squares approach* (Cambridge University Press, 2007).
26. K. Polisano, "Modélisation de textures anisotropes par la transformée en ondelettes monogènes et super-résolution de lignes 2-d," Ph.D. thesis, Université de Grenoble Alpes (2017).
27. F. Brémand, "A phase unwrapping technique for object relief determination," Opt. Lasers Eng. **21**, 49–60 (1994).
28. M. Arevallilo-Herráez, D. R. Burton, M. J. Lalor, and M. A. Gdeisat, "Fast two-dimensional phase-unwrapping algorithm based on sorting by reliability following a noncontinuous path," Appl. Opt. **41**, 7437–7444 (2002).